JACS
JOURNAL OF THE AMERICAN CHEMICAL SOCIETY
Article
Cite This: J. Am. Chem. Soc. 2019, 141, 13948−13953
pubs.acs.org/JACS

Crystalline Liquid-like Behavior: Surface-Induced Secondary Grain Growth of Photovoltaic Perovskite Thin Film

Jingjing Xue,[†,#] Rui Wang,[†,#] Kai-Li Wang,[‡,#] Zhao-Kui Wang,*[,†,‡] Ilhan Yavuz,[§] Yang Wang,[∥] Yingguo Yang,[⊥] Xingyu Gao,[⊥] Tianyi Huang,[†] Selbi Nuryyeva,[†] Jin-Wook Lee,[†] Yu Duan,[†] Liang-Sheng Liao,*[,‡] Richard Kaner,[†] and Yang Yang*[,†]

[†]Department of Materials Science and Engineering and California NanoSystems Institute, University of California Los Angeles, California 90095, United States

[‡]Institute of Functional Nano & Soft Materials (FUNSOM), Jiangsu Key Laboratory for Carbon-Based Functional Materials & Devices, Soochow University, Suzhou 215123, China

[§]Department of Physics, Marmara University, 34722, Ziverbey, Istanbul, Turkey

[∥]School of Chemistry and Chemical Engineering, Yangzhou University, Yangzhou 225002, China

[⊥]Shanghai Synchrotron Radiation Facility (SSRF), Zhangjiang Lab, Shanghai Advanced Research Institute, Chinese Academy of Sciences, Shanghai 201204, China

Supporting Information

ABSTRACT: Surface effects usually become negligible on the micrometer or sub-micrometer scale due to lower surface-to-bulk ratio compared to nanomaterials. In lead halide perovskites, however, their "soft" nature renders them highly responsive to the external field, allowing for extended depth scale affected by the surface. Herein, by taking advantage of this unique feature of perovskites we demonstrate a methodology for property manipulation of perovskite thin films based on secondary grain growth, where tuning of the surface induces the internal property evolution of the entire perovskite film. While in conventional microelectronic techniques secondary grain growth generally involves harsh conditions such as high temperature and straining, it is easily triggered in a perovskite thin film by a simple surface post-treatment, producing enlarged grain sizes of up to 4 μm. The resulting photovoltaic devices exhibit significantly enhanced power conversion efficiency and operational stability over a course of 1000 h and an ambient shelf stability of over 4000 h while maintaining over 90% of its original efficiency.

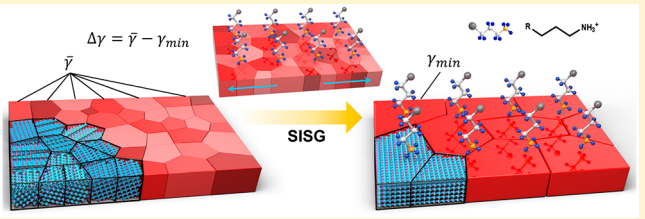

INTRODUCTION

Surface effects play a dominant role in regulating the properties of a solid when the size reaches the nanoscale regime.[1−4] For micrometer or sub-micrometer thin films, which are the most commonly employed thicknesses in the microelectronics industry, the surface effect on the internal properties of the entire film will usually be negligible. However, for "soft" matters such as polymers, or taking the extreme, liquids, due to their highly deformable or flowable character, they can be highly responsive to an external field, upon which the depth scale affected by the surface can dramatically increase to the microscale or even larger.[5−7] Halide perovskite semiconductor materials were recently reported to be inherently "soft"-structured,[8−11] which can be described as a crystalline liquid with both crystalline solid and liquid-like behaviors. The soft nature of halide perovskites offers the possibility of regulating their micrometer-scale thin film behavior via a simple tuning of surface features. Among typical industrial electronic device fabrication techniques, secondary grain growth is a powerful strategy for the fabrication of polycrystalline thin films with grain sizes much larger than the film thickness or even toward single-crystal thin films.[12−16] The resulting reduced grain boundaries not only improve the electronic or photoelectronic behavior but also suppress device degradation pathways resulting from grain boundaries.[17−20] The driving force (ΔF) of secondary grain growth stems from the existence of one or a set of crystallographic textures that minimize the surface free energy such that the grains will grow larger along the orientation to minimize the free energy of the system, which is shown below:[13]

$$\Delta F = F_f - F_i = -\frac{2(\Delta\gamma)}{h} + \frac{\beta\gamma_{gb}}{r}$$

where F_i and F_f is the energy per unit volume before and after the secondary grain growth, respectively; $\Delta\gamma$ is defined as surface energy anisotropy ($\bar{\gamma} - \gamma_{min}$); h is the film thickness; β is a geometric factor (typically equals 0.85 when using a cylinder geometry model); and γ_{gb} is an average grain

Received: June 30, 2019
Published: August 12, 2019

DOI: 10.1021/jacs.9b06940
J. Am. Chem. Soc. 2019, 141, 13948−13953

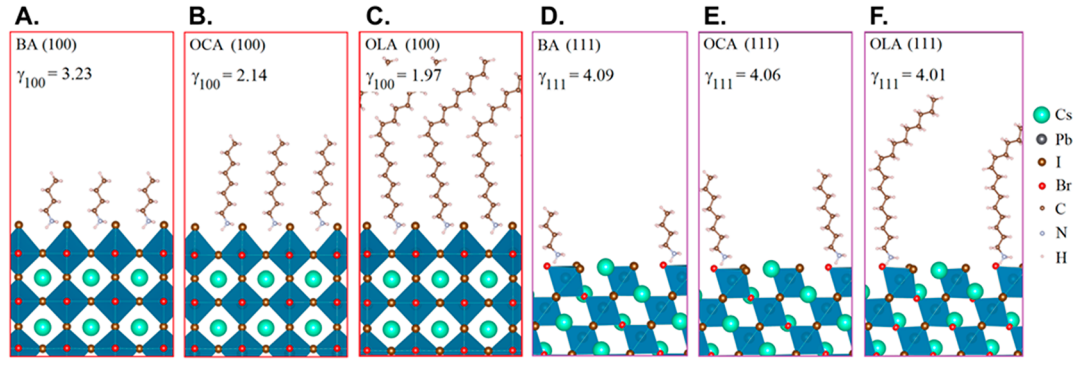

Figure 1. Optimized (100) slab model of perovskite with (A) BA, (B) OCA, (C) OLA termination by DFT-D3 method; optimized (111) slab model of perovskite with (D) BA, (E) OCA, and (F) OLA termination by the DFT-D3 method.

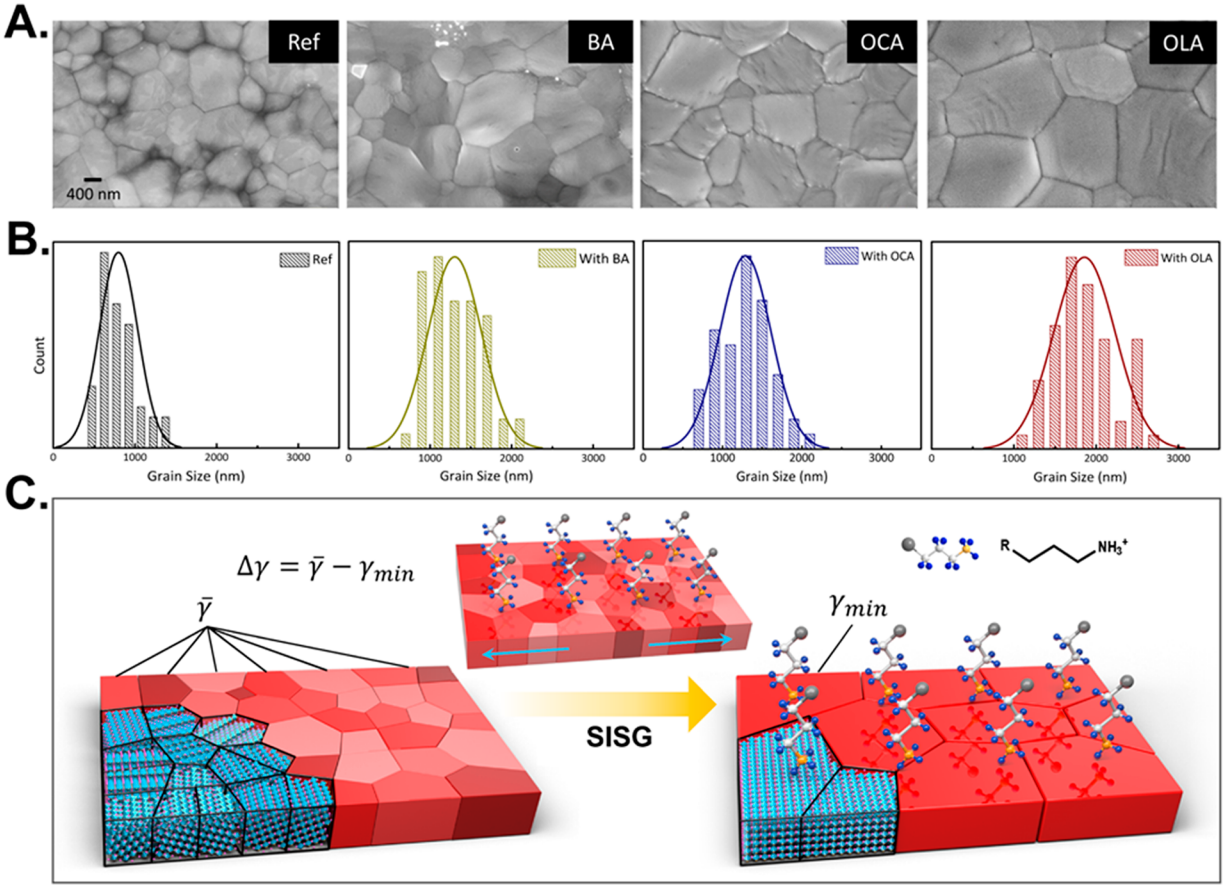

Figure 2. (A) Top-view SEM images of perovskite film with various treatments (IPA, BA, OCA, and OLA). (B) Grain size statistical distribution of perovskite films with various treatments (IPA, BA, OCA, and OLA). (C) Schematic demonstration of the process of surface-induced secondary grain growth.

boundary energy per unit area. The state-of-the-art techniques for secondary grain growth commonly involve harsh and complicated conditions, such as elevated and/or cyclic temperature annealing, chemical doping, and high-pressure plastic straining, to obtain the driving force to trigger grain boundary migration.[21−25] The "soft" liquid-like nature of perovskite offers a way to take advantage of the surface effect on the inner film properties for secondary grain growth. Hence, here we demonstrate a surface-induced secondary grain growth (SISG) technique, where surface modification induces postcrystallization grain growth in the entire perovskite thin film. This strategy sheds light on a new perspective for the perovskite research community, offering a novel methodology for property manipulation of perovskite thin films: changing the surface can induce the property evolution of the perovskite thin film as a whole.

Theoretical Modeling of the Driving Force. For investigation of SISG in perovskite thin films, we chose the $CsPbI_2Br$ perovskite as a model compound, since it is a relatively pure and simple system that contains only inorganic components. Organic components were left out because they will interfere with the elemental analysis and add complexity to the study of chemical interactions in the system, which will obfuscate the investigation of the underlying mechanism.

DOI: 10.1021/jacs.9b06940
J. Am. Chem. Soc. 2019, 141, 13948−13953

Furthermore, compared with the pure iodine-based $CsPbI_3$ perovskite, $CsPbI_2Br$ shows an enhanced phase stability rendering it more promising toward commercialization. For surface manipulation, we chose three organic ammoniums with varying carbon lengths, i.e., *n*-butylammonium (BA), octyl ammonium (OCA), and oleylammonium (OLA), all of which potentially can lower the surface energy of the perovskite (100) plane when anchored to the void of the corner-sharing PbI_6^{4-} octahedron. We first used density functional theory (DFT) to examine the surface energies of the organic ammonium terminated low-index planes of the perovskite based on a slab model (Figure 1 and Table S1; the detailed calculation method can be found in the Supporting Information). The surface free energies of the Cs, BA, OCA, and OLA-terminated (111) planes were found to be similar, while those of the (100) plane were determined to be 4.30, 3.23, 2.14, and 1.97 eV/nm^{-2}, respectively. The surface energy differences between (100) and (111) planes are summarized in Figure S1, demonstrating an increasing surface energy anisotropy in the following order: Cs, BA, OCA, and OLA. This indicated a corresponding increasing driving force for the secondary grain formation.

Characterizations of the Grain Growth and Film Properties. Following theoretical predictions, the three organic ammoniums were evaluated in the preparation of perovskite films via a sequential two-step procedure. $CsPbI_2Br$ perovskite film was fabricated using a one-step method consisting of spin-coating $PbI_2/PbBr_2/CsI$ mixed perovskite precursors on the substrate followed by annealing at 300 °C for 10 min. The substrate was then cooled to room temperature, yielding a black perovskite thin film, which indicates the formation of the $CsPbI_2Br$ cubic phase. For the targeted film, an ammonium iodide isopropanol solution was subsequently spin-coated onto the crystallized perovskite thin film followed by heating to 100 °C for 5 min to remove the excess solvent. For the reference film, pure isopropanol was spin-coated onto perovskite film followed by the same annealing process as the organic ammoniums to examine the effect of isopropanol and heat. The scanning electron microscopy (SEM) images of the fabricated films are shown in Figure 2A. Crystal grains in the reference film were of almost the same size as the ones in the as-fabricated film without any post-treatment (Figure S2), indicating that isopropanol and heat did not induce the grain growth of perovskite. However, films that underwent surface treatment using organic ammoniums showed much enlarged grains. The average grain sizes of films with different post-treatment conditions shown in Figure 2B are 769, 1277, 1287, and 1846 nm for reference, BA, OCA, and OLA, respectively. We attribute this secondary grain growth process to the decrease in surface energy of a crystal facet that provides the driving force of surface anisotropy $\Delta\gamma$. On one hand, the grain had an orientation, i.e., plane (100), that could minimize the surface energy of the film due to the existence of the organic ammonium on the surface. On the other hand, the low activation barrier of ion diffusion in perovskite facilitated by soft lattice modes can facilitate the grain boundaries' rearrangement during the out-of-plane crystalline reorientation process (the orientation will be further discussed in detail).[10] From another aspect, the highly anharmonic lattice with low-frequency modes and small elastic modulus renders the perovskite highly "flowable" and, thus, highly responsive to the influence from the surface.[10,26] Thus, the original perovskite grains were able to grow further in that favorable direction to reduce the energy of the whole system (Figure 2C). The lower the surface energy, the larger the grain could grow. As a result, OLA, which gave the lowest surface energy, induced secondary grain growth with the largest resulting average grain size of up to 4 μm (Figure S3). A mutiphase field model was also employed to simulate the grain growth for the film with and without OLA, which showed a significant increase of the grain size for the film with OLA (Figure S4). This demonstrates that SISG is a powerful strategy toward precise control of perovskite grain size or even perovskite single-crystal thin film given that the surface energy is rationally manipulated.

In situ real time grazing-incidence wide-angle X-ray scattering (GIWAXS) was performed to obtain an in-depth insight into the SISG of the perovskite thin film. The X-ray diffraction signal measurement was initiated once the organic ammonium isopropanol solution was drop-cast onto the pristine perovskite thin film triggering the SISG (Figure S5). Figure 3A shows the time-dependent diffraction peak evolution

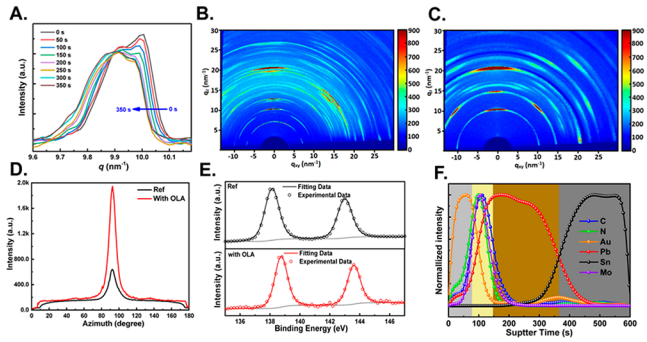

Figure 3. (A) Evolution of the (100) peak position of perovskite film with OLA extracted from real-time in situ GIWAXS measurement. (B and C) 2D GIWAXS patterns of perovskite films (B) without OLA treatment and (C) with OLA treatment. (D) Radially integrated intensity plots along the (100) crystal plane from the 2D GIWAXS patterns in perovskite films with or without OLA treatment. (E) XPS data for Pb 4f 7/2 and Pb 4f 5/2 core level spectra in perovskite films with or without OLA treatment. (F) Time-of-flight secondary ion mass spectroscopy (TOF-SIMS) depth profile of perovskite film with OLA treatment.

at a q_z value of around 10 nm^{-1}, which is a characteristic peak corresponding to the (100) plane of the cubic phase of perovskite.[27] During the SISG process, the peak position gradually shifted to a lower q_z value, indicating a gradual decrease in lattice constant that possibly results from the strain relaxation during the grain growth. The initial peak splitting phenomenon can be attributed to the partial halide segregation in perovskite, which was commonly observed in the $CsPbI_2Br$ film.[28] At a later stage, the dual-peak behavior gradually disappeared, suggesting that the SISG that caused the strain relaxation, as well as better crystallinity of the secondary perovskite grains, might also suppress the halide segregation, which could be beneficial to the long-term stability of the perovskite device (more details will be provided in the device description part).[28] Such a phenomenon was not observed in the reference film eliminating the effect of solvent and heat on the grain size growth in the perovskite film (Figure S6). Figure 3B and C show the two-dimensional GIWAXS patterns of the perovskite film with and without SISG, respectively. The azimuth angle plots in Figure 3D were obtained from the

DOI: 10.1021/jacs.9b06940
J. Am. Chem. Soc. 2019, 141, 13948−13953

patterns by cutting along the (100) plane of the perovskite films. At the azimuth angle of 90°, the perovskite film with SISG showed a very sharp peak with a half-peak width of 9.30°, much lower than that of the reference film (10.66°), demonstrating that SISG produced a more preferred out-of-plane orientation of the secondary perovskite grains. This is consistent with the growth mechanism we proposed earlier suggesting that the presence of organic ammonium on the surface lowers the surface energy of the (100) plane of perovskite and generates a driving force for the grain growth in that direction to minimize the energy of the system. High-resolution X-ray photoelectron spectroscopy (XPS) patterns of the Pb 4f of the reference and targeted films are shown in Figure 3E. For the targeted film, two main peaks located at 138.14 and 143.00 eV were observed corresponding to the Pb 4f 7/2 and Pb 4f 5/2, respectively. For comparison, the reference film showed two main peaks at 138.76 and 143.42 eV. The peaks from Pb 4f shifted to higher binding energies in the film after the SISG process based on OLA, indicating the interaction between organic ammonium on the surface and the Pb in the perovskite lattice.[29] The spatial distribution of OLA in the perovskite film with SISG was characterized by time-of-flight secondary-ion mass spectrometry (TOF-SIMS) with a device structure of ITO/SnO_2/perovskite/MoO_x/Au. As shown in Figure 3F, the C and N profiles, which are the characteristic signals of OLA, exhibited a very narrow distribution (similar to the depth profile of Mo) with little overlap with the depth profile of Pb, which is a representative signal of perovskite. This signifies the existence of OLA only on the surface of the perovskite. The resulting organic ammonium-terminated perovskite film with SISG was further confirmed to have a lower surface energy (38.38 mN/m) than the reference film (59.78 mN/m) via contact angle measurements (Figure S7 and Table 2). In order to further evaluate the perovskite film quality, the X-ray diffraction patterns of the perovskite film after the SISG process based on OLA were obtained (Figure S8). They exhibited much higher peak intensity than that of the reference, suggesting enhanced crystallinity of the secondary perovskite grains. The UV−vis absorption spectrum (Figure S9) demonstrates that the perovskite film with SISG showed higher absorption than the reference, which can be attributed to the enlarged grain sizes and thus enhanced light scattering.[30] The perovskite film after the SISG process exhibits much improved film quality necessary for enhancing the device performance.

Device Performance and Stability. We further assessed the photovoltaic performance of the perovskite films prepared with and without the SISG process by fabricating devices with the ITO/SnO_2/perovskite/PTAA/Au configuration, wherein PTAA refers to poly[bis(4-phenyl)(2,4,6-trimethylphenyl)-amine]. Current density−voltage (J−V) curves of the photovoltaic devices with and without SISG are compared in Figure 4A, in which the highest power conversion efficiency (PCE) of the target device reached 16.58% with negligible hysteresis (open circuit voltage (V_{OC}): 1.23 V, short circuit current (J_{SC}): 16.85 mA cm^{-2}, fill factor (FF): 0.80), while a PCE of only 13.09% was achieved with the control device (V_{OC}: 1.11 V, J_{SC}: 15.32 mA cm^{-2}, FF: 0.77). To the best of our knowledge, this is the highest PCE reported in the $CsPbI_2Br$ system. External quantum efficiency (EQE) spectra of the devices were compared in Figure S10A. An integrated J_{SC} of 16.44 mA cm^{-2} from the target device matched well with the value measured from the J−V scan (<5% discrepancy), while a

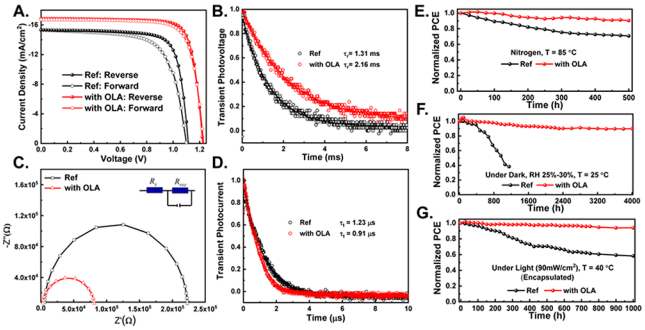

Figure 4. (A) Current density−voltage (J−V) curves of perovskite solar cells with or without OLA treatment. (B) Normalized transient photovoltage decay of perovskite solar cells with or without OLA treatment. (C) Nyquist plots of perovskite solar cells with or without OLA treatment measured in the dark and at corresponding open-circuit voltages. (D) Normalized transient photocurrent decay of perovskite solar cells with or without OLA treatment. (E) Evolution of power conversion efficiency (PCE) of perovskite solar cells with or without OLA treatment. The devices were stored under nitrogen with controlled temperature (85 °C). (F) Evolution of PCE of perovskite solar cells with or without OLA treatment. The devices were stored under dark with controlled humidity. (G) Evolution of the PCEs measured from the encapsulated perovskite solar cells with or without OLA treatment exposed to continuous light (90 ± 5 mW cm^{-2}) under open-circuit conditions.

control device showed an integrated J_{SC} of 14.98 mA cm^{-2}. A stabilized PCE of 16.04% was achieved with the target device when biased at 1.06 V, while that of the control device was 12.36% when biased at 0.94 V (Figure S10B). The remarkably enhanced V_{OC} (by up to 0.12 V) in the device based on SISG can be attributed to the enlarged grain size and, thus, decreased grain boundaries, which usually provide a nonradiative recombination pathway for the carriers due to trap states.[20,31] This is consistent with the transient photovoltage measurements (TPV) under open-circuit condition. As shown in Figure 4B, the device based on SISG exhibited a photovoltage decay time constant of 2.16 ms, which was longer than that of the reference device (1.31 ms), indicating less nonradiative recombination sites.[32] In addition, electrochemical impedance spectroscopy (EIS) characterization was performed to demonstrate the carrier transport processes under illumination at the interface (Figure 4C). The middle frequency zone of the EIS semicircle should be dominated by the junction capacitance and recombination resistance related to the interfaces between the transport materials and the perovskite. According to Figure 4C, the SISG-based device has a smaller impedance than that of the reference, signifying a substantial suppressed recombination at the interface, which most probably originates from the preferred orientation of the perovskite secondary grains that enable improved carrier flow between perovskites and carrier transport layers.[33] Moreover, the hydrophobic tails of the OLAs on the surface of the perovskite could enhance the compatibility of the surface with the upper layer, PTAA, resulting in a better interfacial contact. The improved carrier dynamics can also be reflected in the measurement of transient photocurrent decay. As shown in Figure 4D, the device with SISG had a shorter decay time constant of 0.91 μs compared to that of the reference device (1.23 μs), suggesting a faster carrier collection efficiency, which is consistent with the improved J_{SC} in the targeted device.[32]

DOI: 10.1021/jacs.9b06940
J. Am. Chem. Soc. 2019, 141, 13948−13953

Not only does the photovoltaic efficiency significantly benefit from the SISG strategy, but also the device stability showed remarkable improvement in all aspects, including thermal stability, phase stability, and, thus, operational stability. In Figure 4E, the changes in PCE of the unencapsulated devices in a nitrogen atmosphere at 85 °C were tracked over time to test the long-term thermal stability. While the reference device degraded by 30% in 500 h, the target device maintained 90% of its initial efficiency during this time. Although the all-inorganic perovskite has been reported to show superior thermal and light stability to that of their organic−inorganic counterparts, it is well known to suffer from a rapid phase transition to the non-perovskite phase, especially when exposed to moisture in ambient atmosphere.[28] However, the phase stability of the device based on SISG was noticeably enhanced, maintaining over 90% of its original PCE when stored under ambient conditions with 20−30% humidity at 25 °C for 4000 h. In contrast, the reference device lost >50% of its initial efficiency within 900 h (Figure 4F). The operational stability of the devices was also compared in Figure 4G. The reference device underwent fast degradation, while the device based on SISG maintained >90% of its initial efficiency over the course of 1000 h. Generally, we attribute the dramatically improved stability to two factors resulting from the SISG processing. On one hand, high-quality perovskite films with reduced grain boundaries and higher crystallinity suppress the degradation pathways either through grain boundaries or ion migration, which is also one of the motivations toward single-crystal perovskite thin films.[34] On the other hand, the hydrophobic nature of the small molecules shields the interface from moisture. Therefore, the SISG strategy demonstrates a good example of the possibility to affect and regulate the properties of the entire thin film by tuning of surface states. The surface agents can play a dual functional role of enabling the evolution of the underlying film properties and regulating the interface at the same time to produce improved interfacial contact with the upper layer and thus enabling improvement in both device performance and stability.

To demonstrate the universality of this strategy, we further applied it to the organic−inorganic hybrid perovskite system. As shown in Figure S11 and Figure S12, the post-treatment of OLA can induce the secondary grain growth in the methylammonium (MA)-based formamidinium (FA)-based perovskite thin film as well. The surface energies of the low-index planes of FA-based perovskite with and without OLA were investigated computationally to confirm that the (100) plane became more energy favorable after the surface treatment (Figure S13). The resulting photovoltaic devices showed an improved PCE from 20.04% to 22.13% (Figure S14).

CONCLUSION

The demonstration of surface-state-tuning enabling secondary grain growth over the entire perovskite thin film sheds light on a new research angle in the area of perovskite thin films in regard to surface states by taking advantage of the unique soft nature of perovskites. In contrast to the widely reported strategies of regulating the properties of perovskite thin films via composition tuning, additive incorporation, solvent engineering, and so on, a new methodology basis is proposed: changing the surface is a powerful tool to induce the property evolution of the entire perovskite thin film. Since the surface treatment process is after the formation of the perovskite film, it strategically avoids the limitation of conventional methods in choosing agents/additives that are appropriate with high annealing temperatures of crystallization. Additionally, many of the additives incorporated into perovskite precursors to control the nucleation/growth kinetics, which is often a requirement for high-quality films, always serve as carrier recombination or degradation centers due to the heterogeneous microstructure In contrast, the surface agents that did not penetrate into the perovskite bulk film will not induce the formation of these undesirable centers within the perovskite film. Furthermore, the surface agents provide a versatile platform to tune the interface between the perovskite film and the top layer, which can be regarded as a bifunctional interfacial agent. On one hand, they induce the evolution of the perovskite layer at the bottom, and on the other hand, they serve as an interconnecting layer that improves the contact with the upper layer. Moreover, the utilization of our methodology does not have to be limited to mechanical properties, in which perovskites exhibit low elastic modulus as a reflection of their "soft" nature as demonstrated in this report. We expect the reach of this strategy to extend to the properties in all aspects, such as electronic properties, in which perovskites exhibit low electric modulus, rendering them highly vulnerable to an electric field.[35] A possible example might be introducing surface dipoles to modify the internal electric field and, thus, change the energy levels/band structures of the thin films as a whole. Hence, we hope this strategy will provide a new direction toward high-quality perovskite thin films with tunable and desirable properties and pave the way to the commercialization of perovskite photoelectric devices.

ASSOCIATED CONTENT

Supporting Information

The Supporting Information is available free of charge on the ACS Publications website at DOI: 10.1021/jacs.9b06940.

Experimental details, Supplementary Notes S1−S4, Figures S1−S17, and Tables S1−S7 (PDF)

AUTHOR INFORMATION

Corresponding Authors

*zkwang@suda.edu.cn
*lsliao@suda.edu.cn
*yangy@ucla.edu

ORCID

Zhao-Kui Wang: 0000-0003-1707-499X
Ilhan Yavuz: 0000-0002-3268-6268
Yang Wang: 0000-0003-2540-2199
Yingguo Yang: 0000-0002-1749-2799
Xingyu Gao: 0000-0003-1477-0092
Yu Duan: 0000-0002-2155-7188
Liang-Sheng Liao: 0000-0002-2352-9666
Richard Kaner: 0000-0003-0345-4924
Yang Yang: 0000-0001-8833-7641

Author Contributions

#J.X., R.W., and K.-L.W. contributed equally.

Notes

The authors declare no competing financial interest.

ACKNOWLEDGMENTS

Y.Y. acknowledges the Office of Naval Research (ONR) (grant no. N00014-17-1-2,484), the Air Force Office of Scientific

DOI: 10.1021/jacs.9b06940
J. Am. Chem. Soc. 2019, 141, 13948−13953

Research (AFOSR) (grant no. FA2386-18-1-4094), the UC Solar Program (grant no. MRPI 328368), and Solargiga Energy. Z.K.W. and L.S.L. acknowledge the Natural Science Foundation of China (No. 91733301). This project is also funded by Collaborative Innovation Center of Suzhou Nano Science and Technology, the Priority Academic Program Development of Jiangsu Higher Education Institutions (PAPD), and by the "111" Project of the State Adminstration of Foreign Experts Affairs of China. Part of the computations are performed in the SIMULAB of Marmara University, Physics Department and in the UHEM cluster of Turkey. Y.W. acknowledges the Thousand Talents Plan for the Young Professionals of China. All the authors thank Prof. Qifeng Han, Dr. Dong Meng, Dr. Lei Meng, Mr. Shaun Tan, Mr. Yepin Zhao, and Mr. Shiqi Zheng for helpful discussions during this project.

REFERENCES

(1) Boles, M. A.; Ling, D.; Hyeon, T.; Talapin, D. V. The Surface Science of Nanocrystals. *Nature Materials*; Nature Publishing Group, 2016; pp 141−153.
(2) Carey, G. H.; Abdelhady, A. L.; Ning, Z.; Thon, S. M.; Bakr, O. M.; Sargent, E. H. Colloidal Quantum Dot Solar Cells. *Chem. Rev.* **2015**, *115* (23), 12732−12763.
(3) Milliron, D. J. Quantum Dot Solar Cells: The Surface Plays a Core Role. *Nat. Mater.* **2014**, *13* (8), 772−773.
(4) Diao, J.; Gall, K.; Dunn, M. L. Surface-Stress-Induced Phase Transformation in Metal Nanowires. *Nat. Mater.* **2003**, *2* (10), 656−660.
(5) Ding, Y.; Niu, X. R.; Wang, G. F.; Feng, X. Q.; Yu, S. W. Surface Effects on Nanoindentation of Soft Solids by Different Indenters. *Mater. Res. Express* **2016**, *3* (11), 115021.
(6) Thomas, B.; Jacques, L. O. M.-M. Soft Acoustic Metamaterials. *Science (80-.).* **2013**, *342* (6156), 323−324.
(7) Xu, X.; Jagota, A.; Peng, S.; Luo, D.; Wu, M.; Hui, C. Y. Gravity and Surface Tension Effects on the Shape Change of Soft Materials. *Langmuir* **2013**, *29* (27), 8665−8674.
(8) Zhu, H.; Miyata, K.; Fu, Y.; Wang, J.; Joshi, P. P.; Niesner, D.; Williams, K. W.; Jin, S.; Zhu, X. Y. Screening in Crystalline Liquids Protects Energetic Carriers in Hybrid Perovskites. *Science (Washington, DC, U. S.)* **2016**, *353* (6306), 1409−1413.
(9) Joshi, P. P.; Maehrlein, S. F.; Zhu, X. Dynamic Screening and Slow Cooling of Hot Carriers in Lead Halide Perovskites. *Adv. Mater.* **2019**, *1803054*, 1−10.
(10) Lai, M.; Obliger, A.; Lu, D.; Kley, C. S.; Bischak, C. G.; Kong, Q.; Lei, T.; Dou, L.; Ginsberg, N. S.; Limmer, D. T. Intrinsic Anion Diffusivity in Lead Halide Perovskites Is Facilitated by a Soft Lattice. *Proc. Natl. Acad. Sci. U. S. A.* **2018**, *115* (47), 201812718.
(11) Miyata, K.; Atallah, T. L.; Zhu, X. Y. Lead Halide Perovskites: Crystal-Liquid Duality, Phonon Glass Electron Crystals, and Large Polaron Formation. *Science Advances*; American Association for the Advancement of Science, 2017; p e1701469.
(12) Omori, T.; Kusama, T.; Kawata, S.; Ohnuma, I.; Sutou, Y.; Araki, Y.; Ishida, K.; Kainuma, R. Abnormal Grain Growth Induced by Cyclic Heat Treatment. *Science (Washington, DC, U. S.)* **2013**, *341* (6153), 1500−1502.
(13) Thompson, C. V. Secondary Grain Growth in Thin Films of Semiconductors: Theoretical Aspects. *J. Appl. Phys.* **1985**, *58*, 763.
(14) Ye, Z. G. *Handbook of Advanced Dielectric, Piezoelectric and Ferroelectric Materials: Synthesis, Properties and Applications*; 2008; DOI: 10.1533/9781845694005.
(15) Thompson, C. V. Grain Growth in Thin Films. *Annu. Rev. Mater. Sci.* **1990**, *20*, 245.
(16) Kang, S.-J. L. *Sintering: Densification, Grain Growth, and Microstructure*; 2005, Chapter 3, pp 117-135.
(17) Tsen, A. W.; Brown, L.; Levendorf, M. P.; Ghahari, F.; Huang, P. Y.; Havener, R. W.; Ruiz-Vargas, C. S.; Muller, D. A.; Kim, P.; Park, J. Tailoring Electrical Transport Across Grain Boundaries in Polycrystalline Graphene. *Science (80-.).* **2012**, *336* (6085), 1143−1146.
(18) Seager, C. H.; Ginley, D. S. Passivation of Grain Boundaries in Polycrystalline Silicon. *Appl. Phys. Lett.* **1979**, *34* (5), 337−340.
(19) Liu, Y.; Zhang, Y.; Yang, Z.; Yang, D.; Ren, X.; Pang, L.; Liu, S. F. Thinness- and Shape-Controlled Growth for Ultrathin Single-Crystalline Perovskite Wafers for Mass Production of Superior Photoelectronic Devices. *Adv. Mater.* **2016**, *28* (41), 9204−9209.
(20) Son, D. Y.; Lee, J. W.; Choi, Y. J.; Jang, I. H.; Lee, S.; Yoo, P. J.; Shin, H.; Ahn, N.; Choi, M.; Kim, D. Self-Formed Grain Boundary Healing Layer for Highly Efficient CH3NH3PbI3perovskite Solar Cells. *Nat. Energy* **2016**, *1* (7), 16081.
(21) Thompson, C. V. Structure Evolution During Processing of Polycrystalline Films. *Annu. Rev. Mater. Sci.* **2000**, *30*, 159.
(22) Miller, D. L.; Keller, M. W.; Shaw, J. M.; Rice, K. P.; Keller, R. R.; Diederichsen, K. M. Giant Secondary Grain Growth in Cu Films on Sapphire. *AIP Adv.* **2013**, *3*, 082105.
(23) Palmer, J. E.; Thompson, C. V.; Smith, H. I. Grain Growth and Grain Size Distributions in Thin Germanium Films. *J. Appl. Phys.* **1987**, *62*, 2492.
(24) Ciulik, J.; Taleff, E. M. Dynamic Abnormal Grain Growth: A New Method to Produce Single Crystals. *Scr. Mater.* **2009**, *61* (9), 895−898.
(25) Omori, T.; Kusama, T.; Kawata, S.; Ohnuma, I.; Sutou, Y.; Araki, Y.; Ishida, K.; Kainuma, R. Abnormal Grain Growth Induced by Cyclic Heat Treatment. *Science (Washington, DC, U. S.)* **2013**, *341* (6153), 1500−1502.
(26) Ferreira, A. C.; Létoublon, A.; Paofai, S.; Raymond, S.; Ecolivet, C.; Rufflé, B.; Cordier, S.; Katan, C.; Saidaminov, M. I.; Zhumekenov, A. A., Bakr, O. M., Even, J., Bourges, P. Elastic Softness of Hybrid Lead Halide Perovskites. *Phys. Rev. Lett.* **2018**, *121* (8). DOI: 10.1103/PhysRevLett.121.085502
(27) Nam, J. K.; Chun, D. H.; Rhee, R. J. K.; Lee, J. H.; Park, J. H. Methodologies toward Efficient and Stable Cesium Lead Halide Perovskite-Based Solar Cells. *Advanced Science*; John Wiley & Sons, Ltd, 2018; p 1800509.
(28) Zeng, Q.; Zhang, X.; Liu, C.; Feng, T.; Chen, Z.; Zhang, W.; Zheng, W.; Zhang, H.; Yang, B. Inorganic CsPbI 2 Br Perovskite Solar Cells: The Progress and Perspective. *Sol. RRL* **2019**, *3* (1), 1800239.
(29) Liu, L.; Huang, S.; Lu, Y.; Liu, P.; Zhao, Y.; Shi, C.; Zhang, S.; Wu, J.; Zhong, H.; Sui, M.; Zhou, H.; Jin, H.; Li, Y.; Chen, Q. Grain-Boundary "Patches" by In Situ Conversion to Enhance Perovskite Solar Cells Stability. *Adv. Mater.* **2018**, *30* (29), 1800544.
(30) Im, J. H.; Jang, I. H.; Pellet, N.; Grätzel, M.; Park, N. G. Growth of CH3 NH3 PbI3 Cuboids with Controlled Size for High-Efficiency Perovskite Solar Cells. *Nat. Nanotechnol.* **2014**, *9* (11), 927−932.
(31) Niu, T.; Lu, J.; Munir, R.; Li, J.; Barrit, D.; Zhang, X.; Hu, H.; Yang, Z.; Amassian, A.; Zhao, K.; Liu, S. Stable High-Performance Perovskite Solar Cells via Grain Boundary Passivation. *Adv. Mater.* **2018**, *30* (16), 1706576.
(32) Meng, L.; Sun, C.; Wang, R.; Huang, W.; Zhao, Z.; Sun, P.; Huang, T.; Xue, J.; Lee, J.-W.; Zhu, C.; Huang, Y.; Li, Y.; Yang, Y. Tailored Phase Conversion under Conjugated Polymer Enables Thermally Stable Perovskite Solar Cells with Efficiency Exceeding 21%. *J. Am. Chem. Soc.* **2018**, *140* (49), 17255.
(33) Zheng, G.; Zhu, C.; Ma, J.; Zhang, X.; Tang, G.; Li, R.; Chen, Y.; Li, L.; Hu, J.; Hong, J.; Chen, Q.; Gao, X.; Zhou, H. Manipulation of Facet Orientation in Hybrid Perovskite Polycrystalline Films by Cation Cascade. *Nat. Commun.* **2018**, *9* (1), 2793.
(34) Shao, Y.; Fang, Y.; Li, T.; Wang, Q.; Dong, Q.; Deng, Y.; Yuan, Y.; Wei, H.; Wang, M.; Gruverman, A.; Shield, J.; Huang, J. Grain Boundary Dominated Ion Migration in Polycrystalline Organic-Inorganic Halide Perovskite Films. *Energy Environ. Sci.* **2016**, *9* (5), 1752−1759.
(35) Huang, J.; Yuan, Y.; Shao, Y.; Yan, Y. Understanding the Physical Properties of Hybrid Perovskites for Photovoltaic Applications. *Nat. Rev. Mater.* **2017**, *2*, 17042.

DOI: 10.1021/jacs.9b06940
J. Am. Chem. Soc. 2019, 141, 13948−13953